


Article

Lithium-Cation Conductivity of Solid Solutions in $\text{Li}_{6-x}\text{Zr}_{2-x}\text{A}_x\text{O}_7$ (A = Nb, Ta) Systems

Georgiy Sh. Shekhtman ^{*}, Anastasia V. Kalashnova  and Boris D. Antonov

Institute of High Temperature Electrochemistry, Ural Branch, Russian Academy of Sciences,
20 Akademicheskaya St., 620990 Ekaterinburg, Russia; kalashnova@ihte.uran.ru (A.V.K.);
B.Antonov@ihte.uran.ru (B.D.A.)

* Correspondence: shekhtman@ihte.uran.ru

Abstract: $\text{Li}_{6-x}\text{Zr}_{2-x}\text{A}_x\text{O}_7$ (A = Nb; Ta) system with $0 < x < 0.30$ is synthesized by glycine-nitrate method. Boundaries of solid solutions based on monoclinic $\text{Li}_6\text{Zr}_2\text{O}_7$ are determined; temperature (200–600 °C) and concentration dependences of conductivity are investigated. It is shown that monoclinic $\text{Li}_6\text{Zr}_2\text{O}_7$ exhibits better transport properties compared to its triclinic modification. $\text{Li}_{5.8}\text{Zr}_{1.8}\text{Nb}(\text{Ta})_{0.2}\text{O}_7$ solid solutions have a higher lithium-cation conductivity at 300 °C compared to solid electrolytes based on other lithium zirconates due the “open” structure of monoclinic $\text{Li}_6\text{Zr}_2\text{O}_7$ and a high solubility of the doping cations.

Keywords: solid electrolytes; lithium zirconates; lithium cation conductivity; crystal structure; glycine-nitrate synthesis; heterovalent doping



Citation: Shekhtman, G.S.; Kalashnova, A.V.; Antonov, B.D. Lithium-Cation Conductivity of Solid Solutions in $\text{Li}_{6-x}\text{Zr}_{2-x}\text{A}_x\text{O}_7$ (A = Nb, Ta) Systems. *Materials* **2021**, *14*, 6904. <https://doi.org/10.3390/ma14226904>

Academic Editor: Changshin Jo

Received: 13 October 2021

Accepted: 9 November 2021

Published: 16 November 2021

Publisher's Note: MDPI stays neutral with regard to jurisdictional claims in published maps and institutional affiliations.



Copyright: © 2021 by the authors. Licensee MDPI, Basel, Switzerland. This article is an open access article distributed under the terms and conditions of the Creative Commons Attribution (CC BY) license (<https://creativecommons.org/licenses/by/4.0/>).

1. Introduction

Lithium zirconates are a subject of wide-ranging studies during the last years due to the wide range of their practical applications. In particular, their feasibility of using as tritium breeder materials in thermonuclear fusion reactors [1–3], and carbon dioxide sorbents [4,5], has been demonstrated. Besides, lithium zirconates are thermodynamically stable against Li [6], so may be used in lithium power sources. So, attempts have been made to use lithium zirconates as component of electrode mass [7–11] and solid lithium conducting electrolytes [12,13] for various types of lithium batteries. For effective application of lithium zirconates data on their conductivity is of great importance. However, data on lithium zirconates conduction and influence of doping are rather scarce and literature data are contradictory.

According to [14,15], in $\text{Li}_2\text{O}-\text{ZrO}_2$ system form following compounds: Li_2ZrO_3 , $\text{Li}_6\text{Zr}_2\text{O}_7$, and Li_8ZrO_6 . Initial study of Li_2ZrO_3 and Li_8ZrO_6 conductivity revealed that their Li^+ -ion conductivity is $10^{-3}-10^{-4}$ $\text{S}\cdot\text{cm}^{-1}$ at 400 °C and due to their high activation energy they show quick lowering with drop of temperature [12,16]. In more recent publications it was reported that Li_2ZrO_3 near 430 °C transforms into superionic state with sharp rise in ionic conductivity and a heavy drop in activation energy from 98.4 to 13.8 $\text{kJ}\cdot\text{mol}^{-1}$ [17]. A jump-like growth in Li ion conductivity at 400–470 °C was also recorded for Li_8ZrO_6 [18]. For that reason, the authors supposed that both compounds transform into superionic state with disordering of Li^+ sublattice. However, efforts to stabilize high-temperature phases at room temperature by doping, were not successful [19,20]. Besides that, the heavy rise in Li_2ZrO_3 conductivity at 430 °C was not reproduced later [13].

Li^+ ion conductivity of $\text{Li}_6\text{Zr}_2\text{O}_7$ was first measured in [12]. The authors aimed to synthesize Li_4ZrO_4 , but later investigations show that lithium orthozirconate does not exist, and received X-ray patterns earlier ascribed to Li_4ZrO_4 [21] belong to $\text{Li}_6\text{Zr}_2\text{O}_7$ [15]. The conductivity of $\text{Li}_6\text{Zr}_2\text{O}_7$ measured in [12] is rather low: 3.0×10^{-6} $\text{S}\cdot\text{cm}^{-1}$ at 300 °C. However, subsequently it was found that the conductivity of $\text{Li}_6\text{Zr}_2\text{O}_7$ can be considerably increased by heterovalent doping. Thus, when lithium is substituted for divalent

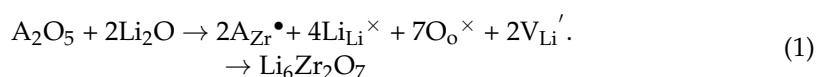
magnesium or zinc cations, the conductivity of the resulting solid electrolytes is 10^{-4} at $300\text{ }^{\circ}\text{C}$ [22]. A more considerable conductivity growth is observed when Zr^{4+} ions are substituted for pentavalent cations (Nb^{5+} or Ta^{5+}) with the positive charge excess compensation by lithium vacancies. Lithium-cation conductivity of $\text{Li}_{5.85}\text{Zr}_{1.85}\text{Ta}_{0.15}\text{O}_7$ solid solution is above $10^{-3}\text{ S}\cdot\text{cm}^{-1}$ at $300\text{ }^{\circ}\text{C}$ [23], (Table 1).

Table 1. Transport properties of $\text{Li}_6\text{Zr}_2\text{O}_7$ and its solid solutions.

Solid Electrolyte	σ_{Li^+} , ($\text{S}\cdot\text{cm}^{-1}$) at $300\text{ }^{\circ}\text{C}$	E_a , (eV)
$\text{Li}_6\text{Zr}_2\text{O}_7$ [12]	3.0×10^{-6}	0.98
$\text{Li}_6\text{Zr}_2\text{O}_7$ [23]	1.2×10^{-5}	1.25
$\text{Li}_6\text{Zr}_2\text{O}_7$ [24]	9.4×10^{-6}	0.84
$\text{Li}_6\text{Zr}_2\text{O}_7$ [22]	10^{-6}	1.07
$\text{Li}_{5.85}\text{Zr}_{1.85}\text{Nb}_{0.15}\text{O}_7$ [23]	1.8×10^{-4}	0.99
$\text{Li}_{5.85}\text{Zr}_{1.85}\text{Ta}_{0.15}\text{O}_7$ [23]	1.7×10^{-3}	0.95

On substitution of Li^+ by double charged ions and on substitution of Zr^{4+} by pentavalent ions Nb^{5+} or Ta^{5+} , charge compensation is accomplished by the creation of lithium vacancies. Electromigration in that kind of solid solutions is realized via the vacancy mechanism, i.e., lithium vacancies are the charge carriers. The amount of vacancies increases with the concentration of the dopant and depends on the range of the single phase region. However, the work [23], investigates only two compositions of solid electrolytes: $\text{Li}_{5.85}\text{Zr}_{1.85}\text{A}_{0.15}\text{O}_7$ ($\text{A} = \text{Nb}, \text{Ta}$). Such high conductivity values obtained in the initial studies give reason to extend study of the conductivity of $\text{Li}_6\text{Zr}_2\text{O}_7$ -based solid solutions in $\text{Li}_{6-x}\text{Zr}_{2-x}\text{Nb}_x\text{O}_7$ and $\text{Li}_{6-x}\text{Zr}_{2-x}\text{Ta}_x\text{O}_7$ systems in the wide concentration region.

The present paper investigates the effect the concentration of pentavalent doping cations in $\text{Li}_{6-x}\text{Zr}_{2-x}\text{A}_x\text{O}_7$ ($\text{A} = \text{Nb}, \text{Ta}$) systems has on the lithium-cation conductivity of $\text{Li}_6\text{Zr}_2\text{O}_7$. It is assumed that when A^{5+} ions replace Zr^{4+} , the compensation of the charge imbalance by lithium vacancies can be described as



2. Materials and Methods

Li_2CO_3 (reagent grade), $\text{Zr}(\text{OH})_2\text{CO}_3 \cdot 5.5\text{H}_2\text{O}$ (analytical grade), and Nb_2O_5 or Ta_2O_5 (analytical grade) all VECTON RF were used as starting reagents to synthesize the substances under study. Lithium carbonate was previously dried at $300\text{ }^{\circ}\text{C}$, niobium and tantalum oxides were annealed at $1000\text{ }^{\circ}\text{C}$.

Several methods of $\text{Li}_6\text{Zr}_2\text{O}_7$ synthesis are described in literature: solid state reaction [15,24–26], co-precipitation of hydroxides [5], a combined method [27]. In [24], solid solutions based on $\text{Li}_6\text{Zr}_2\text{O}_7$ were produced via urea combustion followed by heat treatment. A similar method is used in the present work, except for the fact that instead of urea we use glycine.

The required quantities of the starting reagents were weighed (FX40-CJ analytical balance, Tokyo, Japan BMI Surplus) within the accuracy of $\pm 10^{-4}\text{ g}$ and ground together in a jasper mortar. To compensate for Li_2O loss at heat treatment, a slight (5 wt%) excess of Li_2CO_3 was added to the starting mixtures. The resulting mixtures were dissolved in a water solution of HNO_3 (reagent grade), evaporated under stirring, then glycine ($\text{C}_2\text{H}_5\text{NO}_2$) of analytical purity was added. After portion of water evaporates, the reaction mixtures turn into a syrup-like liquid, which ignites spontaneously at further heating. The powder obtained was calcinated in air at $650\text{ }^{\circ}\text{C}$ for 3 h to remove the organic compounds, then the mixtures were ground and sintered at $850\text{--}950\text{ }^{\circ}\text{C}$ for 8–16 h. The obtained materials were ground into powder with particles less than $50\text{ }\mu\text{m}$ and pressed in stainless

steel die into pellets 10 mm in diameter and 1–1.5 mm thick at 100–300 MPa. The pressed pellets were sintered at 900 °C for 5 h in the powder of the same composition. The density of the sintered pellets was 90–95% of the theoretical.

The phase composition of the samples was studied by XRD on a Rigaku D/MAX-2200VL/PC instrument (RIGAKU, Tokyo, Japan) in filtered Cu K α -radiation generated at 40 kW, 30 mA ($\lambda = 1.54178 \text{ \AA}$) stepwise with 0.3 s counting time and the step of 0.02° at room temperature in air. MDI Jade 6.5 software and PDF-2 ICDD database were used to analyze phase composition and to calculate unit cell parameters. The error of the cell parameters calculation did not exceed 0.02%. The data for full-profile Rietveld analysis in the range of $15^\circ < 2\Theta < 90^\circ$ were recorded with 4 s holding time per step. Crystal structure refinement was performed using the FullProf program [28].

The morphology and microstructure of the material synthesized were examined using MIRA 3 LMU scanning electron microscope (TESCAN, Brno, Czech Republic).

The electrical resistance of the samples was measured in air across 200–600 °C temperature range by P-40xpotentiostat-galvanostat (Elins, Zelenograd, Russia) with FRA-24M module for electrochemical impedance measurements over the frequency range of 50 Hz–500 kHz. Silver applied by a thermochemical method was used as electrodes. The measurements were performed during stepwise cooling with the step of 20 °C. The samples were kept for 15–20 min at every measurement temperature to allow the electric resistance to reach a stable value. The resistance of the samples was determined by analyzing the impedance frequency dispersion. The resultant equivalent circuit is given in Figure 1, where C_g is the geometrical capacity, R_{total} is the resistance of the sample, CPE is the constant phase element reflecting the polarization at the electrode–electrolyte interface. The resistance of the sample in this case is the sum of the volume resistance (R_v) and grain boundary resistance (R_{gb}), i.e., $R_{\text{total}} = R_v + R_{gb}$.

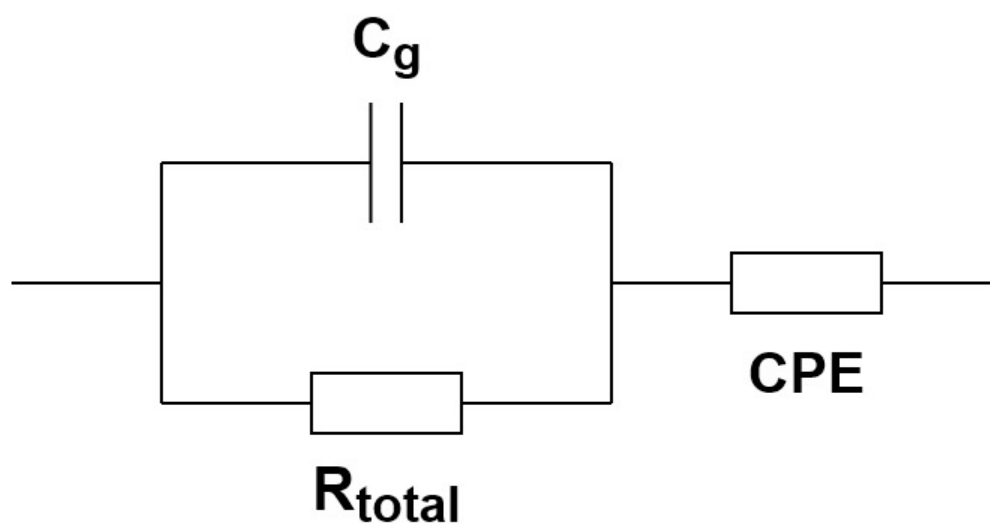


Figure 1. Resultant equivalent circuit for $\text{Ag}_x\text{Li}_{6-x}\text{Zr}_{2-x}\text{Nb}(\text{Ta})_x\text{O}_{7+x}\text{Ag}$ cell.

The impedance spectra for the undoped $\text{Li}_6\text{Zr}_2\text{O}_7$ and for the solid solutions are identical. The spectra for the $\text{Ag} | \text{Li}_{5.95}\text{Zr}_{1.95}\text{Nb}_{0.05}\text{O}_7 | \text{Ag}$ cell at different temperatures are given in Figure 2 as examples. At low temperatures the spectra consist of a semicircular arc in the high-frequency region and a tail in the low-frequency region (Figure 2a).

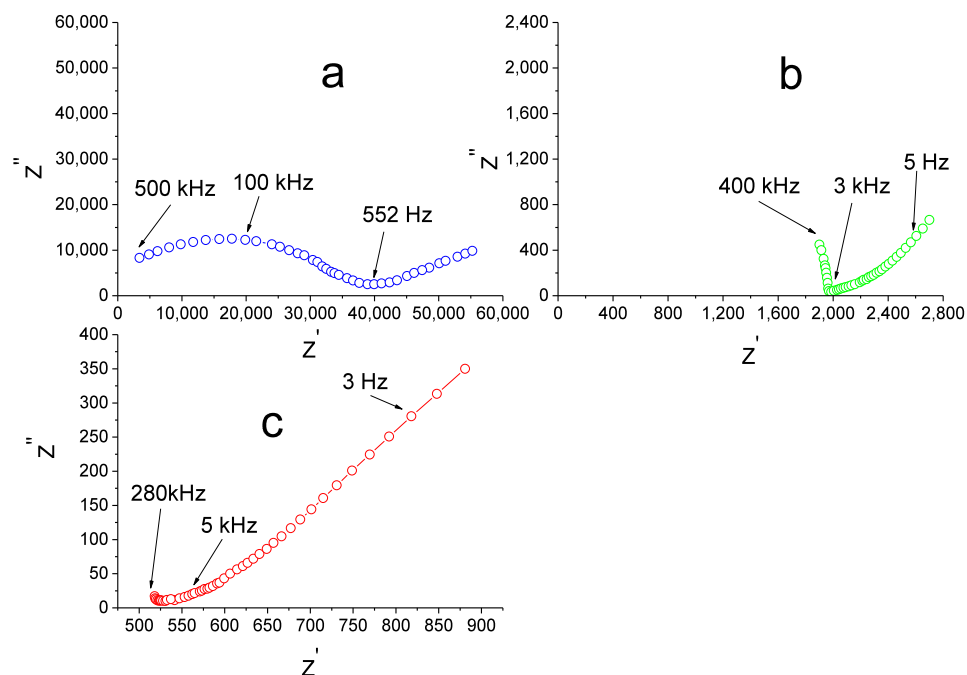


Figure 2. Impedance spectra of Ag | Li_{5.95}Zr_{1.95}Nb_{0.05}O₇ | Ag cell at 225 (a), 400 (b), 550 (c).

The resistance R_{total} of the sample was determined as the value corresponding to the point of intersection between the high-frequency arc and the Z' axis. As the temperature rises, the semicircle becomes smaller (Figure 2b), and above 500–550 °C only a tail is observed across the whole accessible frequency range (Figure 2c). In this case R_{total} was found by the extrapolation of the low-frequency linear portion onto the Z' axis. The corresponding value of specific conductivity was calculated according to the formula:

$$\sigma = l/R_{\text{total}} \cdot S \quad (2)$$

where l is the length of the sample, S is the area of its cross-section.

The electron conductivity was determined using DC method with gold electrodes at 40–50 mV and in all the cases did not exceed 1% of total conductivity.

3. Results and Discussion

The crystal structure of Li₆Zr₂O₇ was studied by X-ray analysis of single crystals [27,29], in [26], the X-ray method was enlarged with the neutron diffraction in order to refine the positions of Li⁺ ions. These data show a good agreement. Li₆Zr₂O₇ has a monoclinic structure, space group C2/c, $a = 10.4428(1)$ Å LATIN CAPITAL, $b = 5.9877(1)$ Å LATIN CAPITAL, $c = 10.2014(1)$ Å LATIN CAPITAL, $\beta = 100.266(1)^\circ$ [25]. The ions of oxygen form a distorted cubic close-packed lattice, in which 1/8 of the sites are vacant. The distribution of lithium and zirconium ions is similar to the distribution of cations in NaCl; besides, zirconium is octahedrally coordinated by oxygen, and Li coordination number is five (a square pyramid).

According to [21], at low temperatures there exists a metastable α -form of Li₆Zr₂O₇, which is produced by annealing the mixture of Li₂CO₃ and ZrO₂ at 850–900 °C and which passes into β -form at high temperatures. The work [15] confirms the existence of α -modification of Li₆Zr₂O₇, which has a triclinic structure with $a = 6.0153(4)$ Å, $b = 9.1941(12)$ Å, $c = 5.3112(6)$ Å, $\alpha = 96.30(1)^\circ$, $\beta = 107.16(1)^\circ$, $\gamma = 89.74(1)^\circ$, however, the authors point out that this phase can only be formed if Li₂CO₃ is used as lithium source. Synthesis at 750 °C produces single-phase Li₆Zr₂O₇ samples with triclinic structure. If the annealing temperature is 800 °C, the triclinic and monoclinic modifications co-exist in the sample, and at higher temperatures the triclinic one disappears. Using ZrO₂ and Li₂O oxides as the starting

components yielded a monoclinic phase irrespective of the synthesis temperature. Thus, the formation of the metastable triclinic modification of $\text{Li}_6\text{Zr}_2\text{O}_7$ via synthesis from Li_2CO_3 and ZrO_2 is confirmed by literature data, but the temperature and the time of heat treatment required to produce single-phase samples with a stable monoclinic structure are quite different in [15,22].

In the present work, the glycine-nitrate stage of $\text{Li}_6\text{Zr}_2\text{O}_7$ synthesis was followed by keeping the reaction mixture at 850, 900, and 950 °C. The results indicate that heat treatment at 850 and 900 °C produces a mixture of triclinic and monoclinic modifications. Notably, if the heat treatment time is increased from 8 to 16 h, the proportion of the triclinic modification decreases. Figure 3 contains Rietveld refinement of the powder XRD pattern for the sample sintered at 900 °C for 8 h. The data indicate that $\text{Li}_6\text{Zr}_2\text{O}_7$ powder is non-single-phase. The main phase is characterized by a monoclinic syngony with space group C2/c (PDF No 88-2213). The impurity phase of the same chemical composition has a triclinic syngony with space group P1 (PDF No 36-0122). The content of the triclinic phase is estimated to be 8.9%.

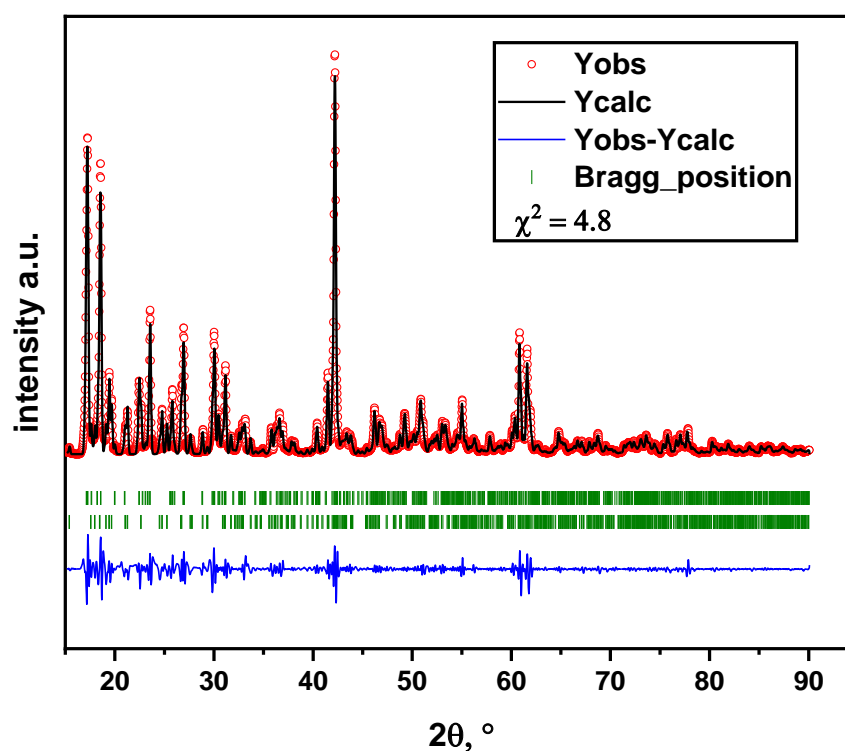


Figure 3. Rietveld refinement of powder XRD pattern for $\text{Li}_6\text{Zr}_2\text{O}_7$ sintered at 900 °C for 8 h. Dots represent the observed data, solid line marks the calculated data. Short green ticks indicate the peak positions of Bragg reflections; the upper row of short green ticks marks the monoclinic phase; the lower row of short green ticks marks the triclinic phase. The bottom line indicates the difference between the calculated and observed data.

The XRD patterns of the samples annealed at 950 °C contain only the reflections of monoclinic $\text{Li}_6\text{Zr}_2\text{O}_7$ (Figure 4), the same applies to the doped samples.

Figure 5 shows SEM images for the surface of $\text{Li}_6\text{Zr}_2\text{O}_7$ sample annealed at 950 °C, as well as for $\text{Li}_{5.8}\text{Zr}_{1.8}\text{Ta}_{0.2}\text{O}_7$ and $\text{Li}_{5.8}\text{Zr}_{1.8}\text{Nb}_{0.2}\text{O}_7$ solid solutions. One can see that the microstructure of the samples is non-homogeneous, and in the case of $\text{Li}_6\text{Zr}_2\text{O}_7$ it consists mainly of particles 0.5–2.0 μm in size (Figure 5a), though some grains are as large as 3 μm . In $\text{Li}_{5.8}\text{Zr}_{1.8}\text{Ta}_{0.2}\text{O}_7$ and $\text{Li}_{5.8}\text{Zr}_{1.8}\text{Nb}_{0.2}\text{O}_7$ the structure is more homogeneous and consists of grains 1–2 μm in size (Figure 5b,c).

It should be pointed out that at temperatures of 900 °C and above lithium oxide is quite volatile, therefore, increasing the temperature and time of heat treatment may cause

a considerable loss of Li_2O . On the other hand, decreasing the temperature results in the formation of triclinic phase in the samples. Thus, a question arises about how the presence of the triclinic modification of $\text{Li}_6\text{Zr}_2\text{O}_7$ affects the conductivity, i.e., what is the relation between the conductivity of the samples having triclinic and monoclinic structure.

Figure 6 shows the temperature dependences of conductivity for $\text{Li}_6\text{Zr}_2\text{O}_7$ samples synthesized at different temperatures. Lines 1 and 2 correspond to the two-phase samples that contain triclinic phase alongside the monoclinic one. It can be assumed from the intensity of the reflections on the XRD pattern, that the content of triclinic phase in sample 1, synthesized at $850\text{ }^\circ\text{C}$, is higher than in sample 2, synthesized at $900\text{ }^\circ\text{C}$. Line 3 corresponds to the single-phase sample with monoclinic structure. Its electric characteristics are close to those given in [12] (Table 1).

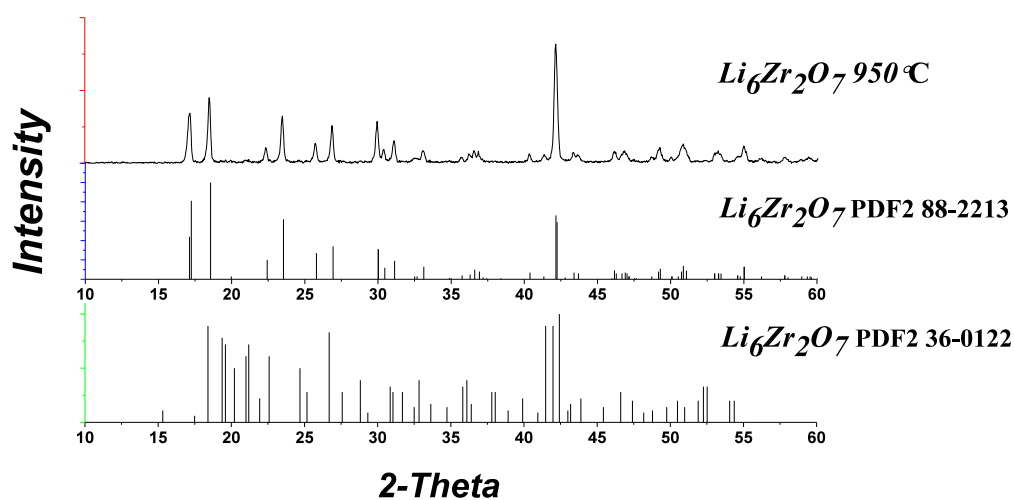
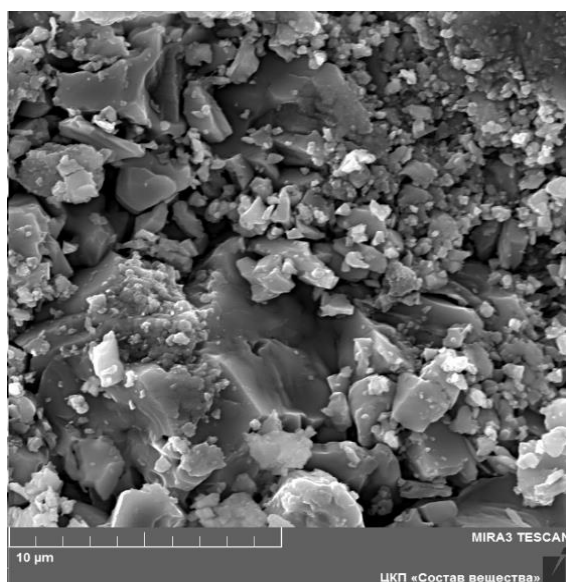
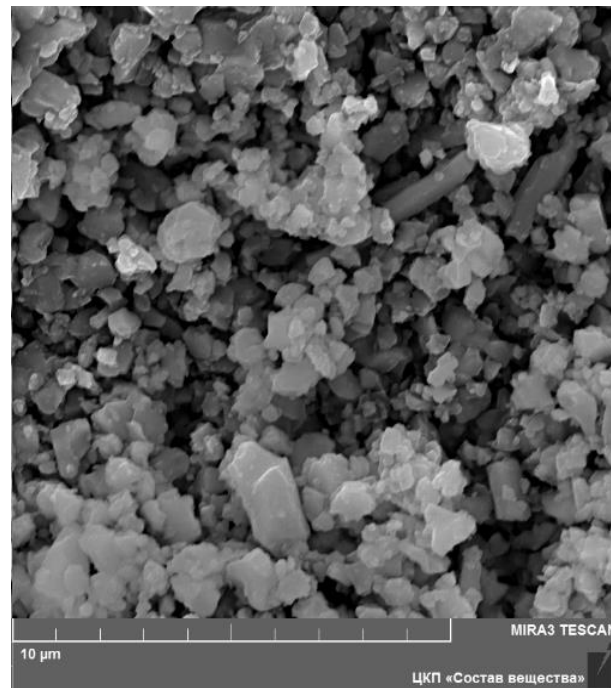


Figure 4. XRD patterns for $\text{Li}_6\text{Zr}_2\text{O}_7$ obtained by glycine-nitrate method from Li_2CO_3 and $\text{Zr}(\text{OH})_2\text{CO}_3 \cdot 5.5\text{H}_2\text{O}$ at $950\text{ }^\circ\text{C}$.

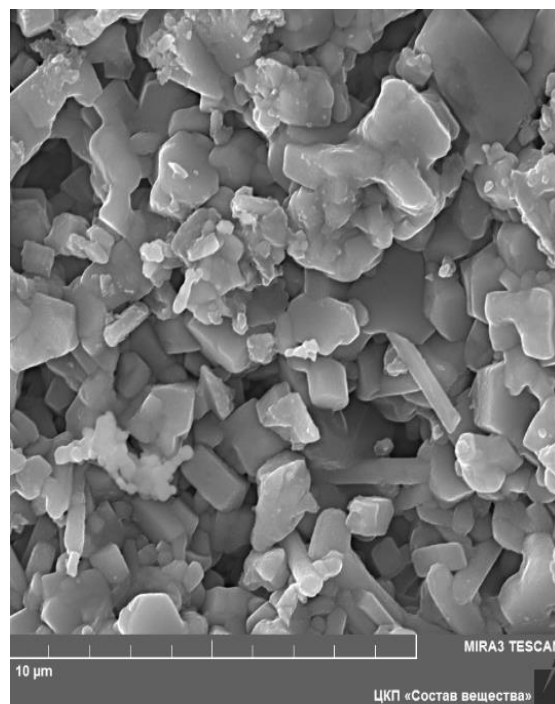


(a)

Figure 5. Cont.



(b)



(c)

Figure 5. SEM images for the surface of $\text{Li}_6\text{Zr}_2\text{O}_7$ (sintered at $950\text{ }^\circ\text{C}$) (a), $\text{Li}_{5,8}\text{Zr}_{1,8}\text{Ta}_{0,2}\text{O}_7$ (b), and $\text{Li}_{5,8}\text{Zr}_{1,8}\text{Nb}_{0,2}\text{O}_7$ sample (c).

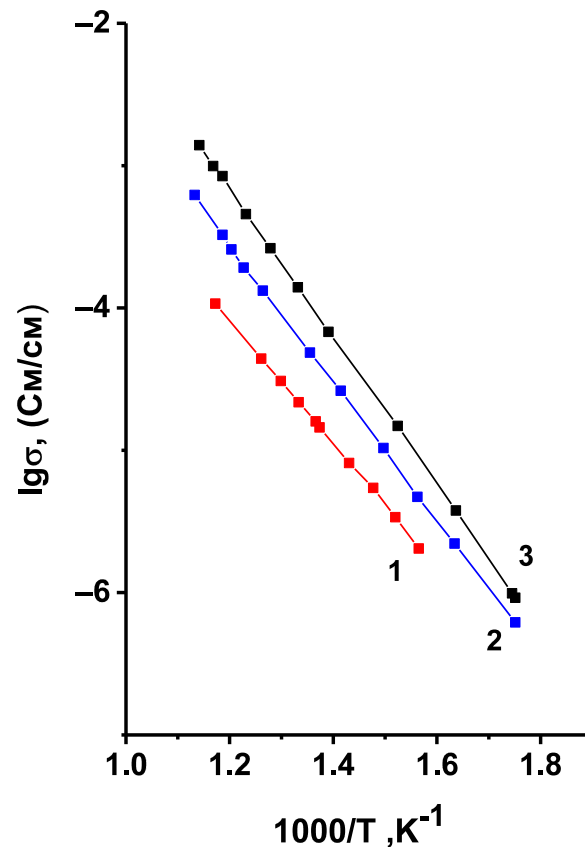


Figure 6. Temperature dependences of conductivity for $\text{Li}_6\text{Zr}_2\text{O}_7$ samples synthesized at 850 °C (1), 900 °C (2), 950 °C (3).

As can be seen from Figure 6, the conductivity of $\text{Li}_6\text{Zr}_2\text{O}_7$ decreases with the appearance of triclinic phase and with the further growth of its content. However, one should take into account that the samples sintered at lower temperatures have a higher porosity, e.g., the porosity of the samples sintered at 850, 900, and 950 °C assessed from saturating the samples with an organic liquid was 24, 19, and 13%, respectively. An increase in the porosity of the samples always leads to a decrease in their conductivity, while the triclinic modification of $\text{Li}_6\text{Zr}_2\text{O}_7$ may have both higher and lower conduction as compared to the monoclinic one. To get reliable data on the relation between the conductivity of triclinic and monoclinic forms of $\text{Li}_6\text{Zr}_2\text{O}_7$, it is necessary to eliminate the effect of porosity. In order to do that we corrected the calculation of conductivity for samples 1, 2, and 3 to the conductivity of non-porous ceramics using the formula for heterogeneous materials [30]:

$$\sigma^* = \sigma_1 \frac{\frac{2\sigma_1 + \sigma_2}{\sigma_2 - \sigma_1} + 2m_2 - \frac{1.65}{\pi} \frac{(\sigma_2 - \sigma_1)}{4\sigma_1 + 3\sigma_2} m_2^{\frac{10}{3}}}{\frac{2\sigma_1 + \sigma_2}{\sigma_2 - \sigma_1} - m_2 - \frac{1.65}{\pi} \frac{3(\sigma_2 - \sigma_1)}{4\sigma_1 + 3\sigma_2} m_2^{\frac{10}{3}}}$$

where σ^* is the measured value of conductivity, σ_1 is the conductivity of the non-porous sample, m_2 is the volume fraction of pores, σ_2 in this case is the conductivity of air, i.e., $\sigma_2 = 0$. The temperature dependences of the corrected conductivity values are given in Figure 7. One can observe here the same tendency for the conductivity to decrease with decreasing synthesis temperature, and, consequently, with the increasing content of the triclinic modification. Thus, across the investigated temperature range the triclinic modification of $\text{Li}_6\text{Zr}_2\text{O}_7$ has a much lower conductivity compared to the monoclinic one, therefore, the final temperature of synthesis for the doped samples was 950 °C, and the absence of the triclinic phase in the synthesized samples was monitored by XRD.

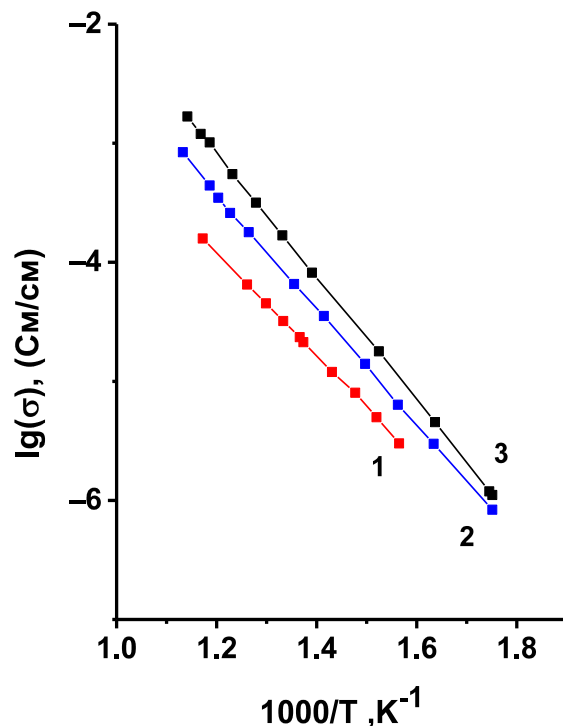


Figure 7. Temperature dependences of $\text{Li}_6\text{Zr}_2\text{O}_7$ conductivity corrected to zero porosity of ceramic samples. The temperature of synthesis and annealing is 850 (1), 900 (2), 950 °C (3).

Phase diagrams for $\text{Li}_2\text{O-ZrO}_2\text{-Nb}_2\text{O}_5$ (Ta_2O_5) systems were investigated in [31], but the authors focused mainly on the study of perovskite-like phases near LiNbO_3 and LiTaO_3 , and, as a result, the domain of $\text{Li}_{6-x}\text{Zr}_{2-x}\text{Nb}(\text{Ta})_x\text{O}_7$ was not considered. According to our results, in both systems under investigation, i.e., $\text{Li}_{6-x}\text{Zr}_{2-x}\text{A}_x\text{O}_7$ ($\text{A} = \text{Nb}, \text{Ta}$), the samples with $0 < x < 0.25$ retain the monoclinic structure of the initial $\text{Li}_6\text{Zr}_2\text{O}_7$ (Figure 8a,b, XRD patterns for $x = 0\text{--}0.20$).

When $x \geq 0.25$, reflections of impurity phases appear on the XRD patterns of the samples, their intensity grows with increasing content of the dopants (Figure 8a,b, XRD patterns for $x = 0.25, 0.30$). In $\text{Li}_{6-x}\text{Zr}_{2-x}\text{Nb}_x\text{O}_7$ system these reflections correspond to the recently investigated $\text{Li}_{29}\text{Zr}_9\text{Nb}_3\text{O}_{40}$ compound [32], (PDF 02-082-2342). The phase appearing in the samples of $\text{Li}_{6-x}\text{Zr}_{2-x}\text{Ta}_x\text{O}_7$ with $x \geq 0.25$ could not be identified using PDF 2, but all the lines that cannot be assigned to $\text{Li}_6\text{Zr}_2\text{O}_7$ practically coincide with the reflections of $\text{Li}_{29}\text{Zr}_9\text{Nb}_3\text{O}_{40}$. Taking into account the closeness of chemical properties that have niobium and tantalum and close values of ionic radii for Nb^{5+} and Ta^{5+} , we can assume that there exists a tantalum analog isostructural with $\text{Li}_{29}\text{Zr}_9\text{Nb}_3\text{O}_{40}$. The results of XRD analysis for the samples of the systems studied are listed in Table 2.

Table 2. Phase composition of $\text{Li}_{6-x}\text{Zr}_{2-x}\text{A}_x\text{O}_7$ ($\text{A} = \text{Nb}, \text{Ta}$) samples according to XRD.

A	X					
	0.05	0.10	0.15	0.20	0.25	0.30
Nb	ss	ss	ss	ss	ss + $\text{Li}_{29}\text{Zr}_9\text{Nb}_3\text{O}_{40}$	ss + $\text{Li}_{29}\text{Zr}_9\text{Nb}_3\text{O}_{40}$
Ta	ss	ss	ss	ss	ss + ?	ss + ?

ss indicates solid solutions with the monoclinic structure of $\text{Li}_6\text{Zr}_2\text{O}_7$.

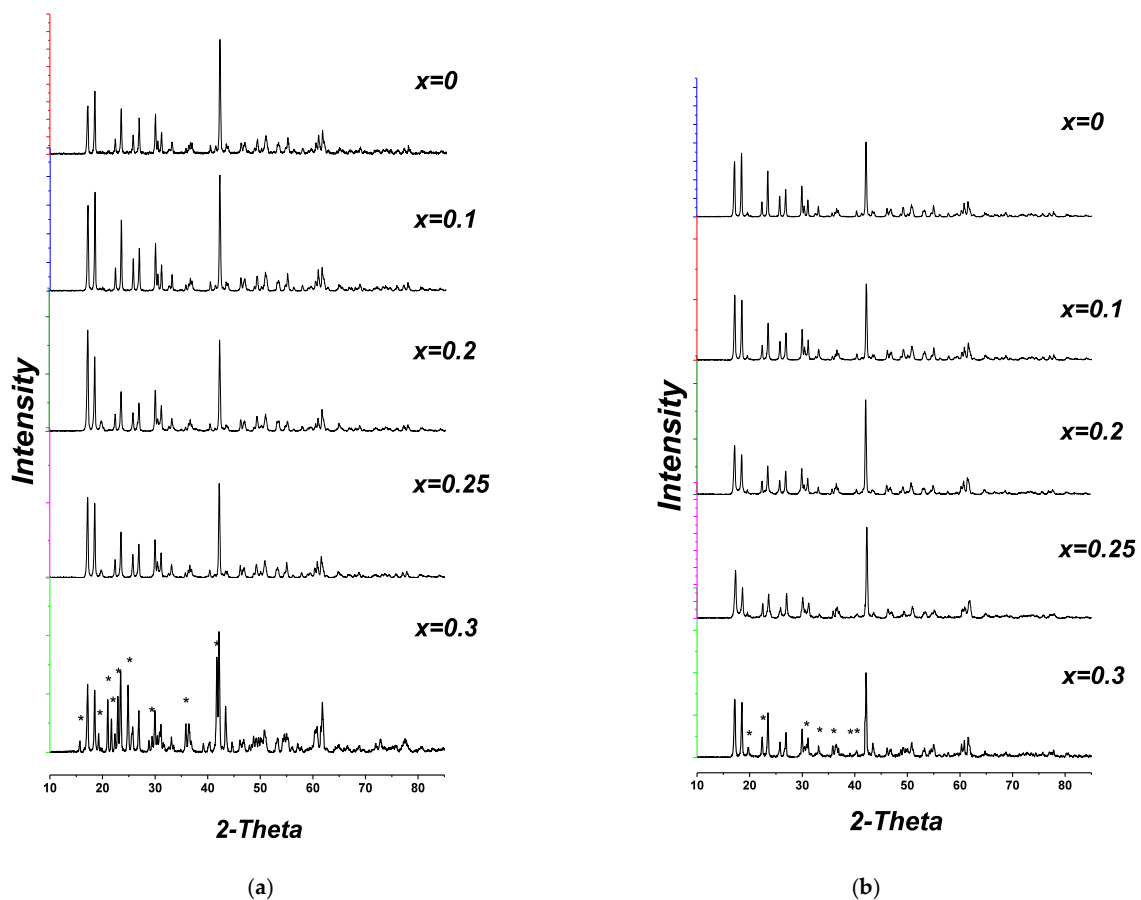


Figure 8. XRD patterns for the samples in $\text{Li}_{6-x}\text{Zr}_{2-x}\text{A}_x\text{O}_7$ system, A = Nb (a), Ta (b).

The plots of concentration vs. the volumes of elementary cells for the phases with monoclinic C2/c structure in the systems investigated are given in Figure 9. The radii of Nb^{5+} and Ta^{5+} ions are practically the same (0.78 Å), but they are slightly smaller than Zr^{4+} (0.86 Å) [33], therefore, the volumes of the elementary cells decrease with the growth of A^{5+} content, and for the samples with the same value of x in the systems with niobium and tantalum their values are close. Overall, the plots of V vs. x correlate with the results of the phase composition studies (Table 2).

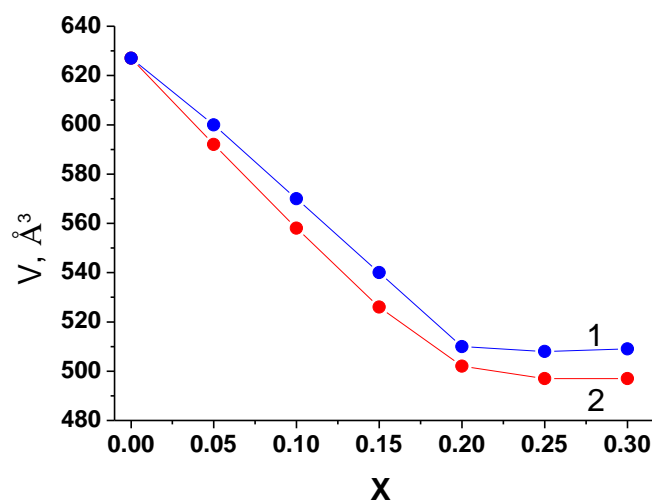


Figure 9. Concentration dependence of the volume of elementary cells in the monoclinic solid solutions of $\text{Li}_{6-x}\text{Zr}_{2-x}\text{Nb}_x\text{O}_7$ (1) and $\text{Li}_{6-x}\text{Zr}_{2-x}\text{Ta}_x\text{O}_7$ (2).

The Arrhenius plots of specific conductivity in both systems studied are linear (Figure 10). The maximum conductivity values in both cases correspond to the samples on the boundaries of single-phase regions (Figure 11, Table 2), i.e., to $\text{Li}_{5.8}\text{Zr}_{1.8}\text{Nb}(\text{Ta})_{0.2}\text{O}_7$.

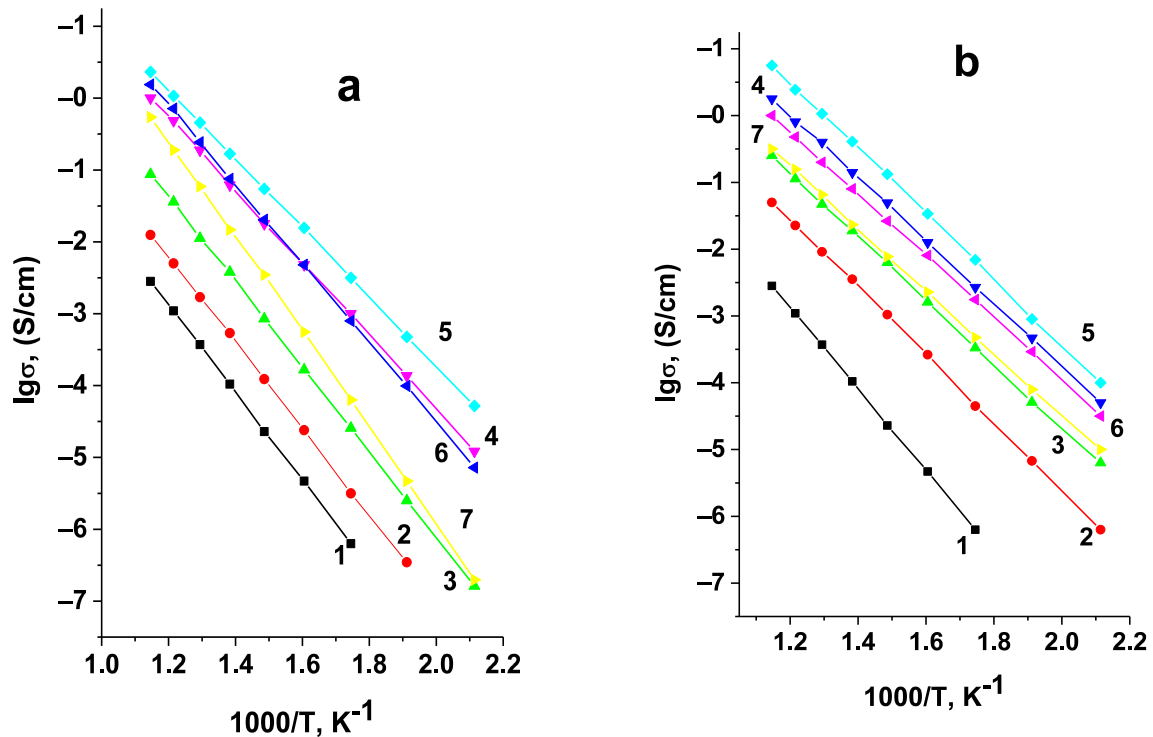


Figure 10. Arrhenius plots for conductivity of $\text{Li}_{6-x}\text{Zr}_{2-x}\text{A}_x\text{O}_7$ A = Nb (a), Ta (b); x = 0(1); 0.05(2); 0.10(3); 0.15(4); 0.20(5); 0.25(6); 0.30(7).

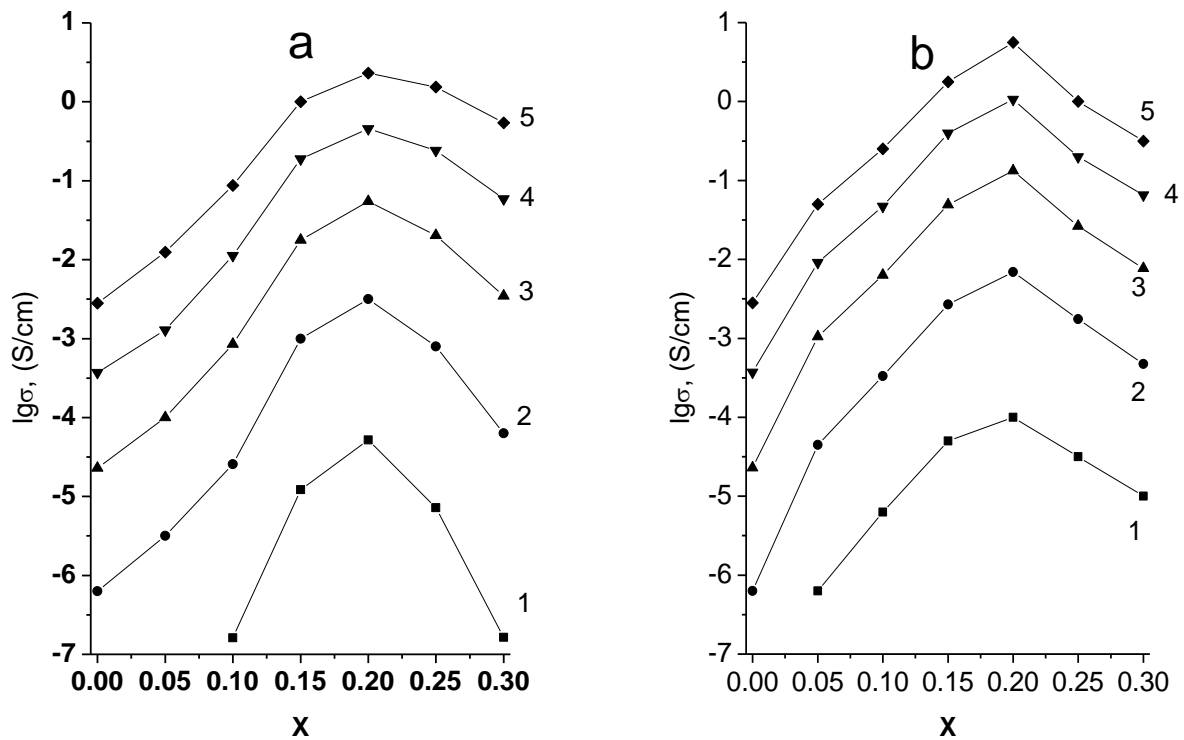


Figure 11. Conductivity isotherms of $\text{Li}_{6-x}\text{Zr}_{2-x}\text{A}_x\text{O}_7$ A = Nb (a), Ta (b). 1–200; 2–300; 3–400; 4–500; 5–600 °C.

The appearance of impurity phases when $x \geq 0.25$ is accompanied by a drop of conductivity in both systems. The conductivity of $\text{Li}_{5.8}\text{Zr}_{1.8}\text{Ta}_{0.2}\text{O}_7$ is $6.92 \times 10^{-3} \text{ S} \times \text{cm}^{-1}$ at 300°C , which is approximately four times higher than the conductivity of $\text{Li}_{5.85}\text{Zr}_{1.85}\text{Ta}_{0.15}\text{O}_7$ reported in [23] ($1.7 \times 10^{-3} \text{ S} \times \text{cm}^{-1}$ at the same temperature), which is explained by a higher content of Ta^{5+} and, consequently, a higher concentration of charge carriers, i.e., lithium vacancies. The conductivity of $\text{Li}_{5.85}\text{Zr}_{1.85}\text{Nb}_{0.15}\text{O}_7$ given in [23], is by an order of magnitude lower than the one of the tantalum-containing sample with the same dopant concentration, which is not quite understandable considering the similarity of the ionic radii, electronegativities, and other characteristics of niobium and tantalum that may affect the conductivity of solid solutions. In the present work, the ionic conductivity of $\text{Li}_{5.8}\text{Zr}_{1.8}\text{Nb}_{0.2}\text{O}_7$ sample was found to be $3.16 \times 10^{-3} \text{ S} \times \text{cm}^{-1}$ at 300°C , which is close to the conductivity of tantalum-containing sample of the same composition.

Solid electrolytes with maximum conductivity in the investigated systems have the lowest activation energy (Figure 12). In the systems with niobium and tantalum these values are similar and equal approximately 1.01 eV, which is close to the values given in literature for vacancy solid solutions based on $\text{Li}_6\text{Zr}_2\text{O}_7$ [23,25].

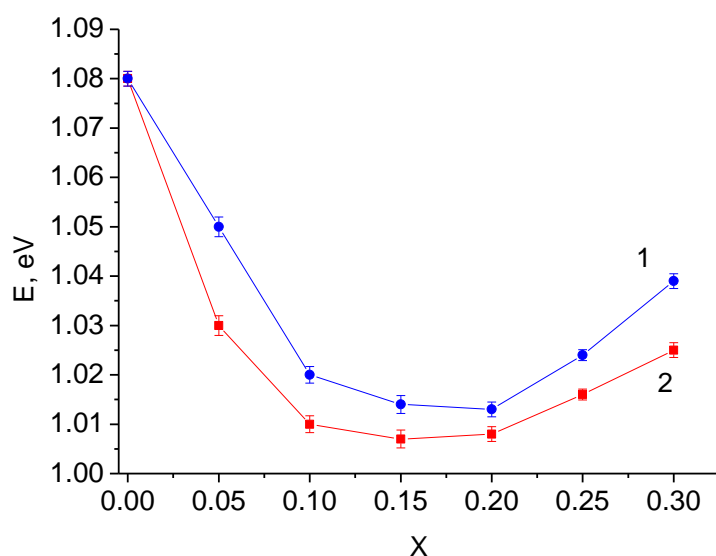


Figure 12. Concentration dependence of activation energy for $\text{Li}_{6-x}\text{Zr}_{2-x}\text{A}_x\text{O}_7$ A = Nb (1), Ta (2).

Table 3 contains transport properties of the materials investigated in the present paper compared to the properties of other solid electrolytes based on lithium zirconates. One can see that $\text{Li}_{5.8}\text{Zr}_{1.8}\text{Nb}(\text{Ta})_{0.2}\text{O}_7$ solid solutions have the highest lithium-cation conductivity at 300°C compared to electrolytes based on Li_2ZrO_3 [34], Li_8ZrO_6 [20,34], and $\text{Li}_6\text{Zr}_2\text{O}_7$ -based solid solutions that form when lithium is substituted for double-charged cations [22], or when zirconium is substituted for triple-charged cations [24]. It should be noted, however, that the activation energy of $\text{Li}_{6.15}\text{Zr}_{1.85}\text{Y}(\text{In})_{0.15}\text{O}_4$ interstitial solid solution is much lower compared to vacancy solid solution based on $\text{Li}_6\text{Zr}_2\text{O}_7$ (Table 3). The authors of [24] assign this to the fact that the coulombic interaction between Li^+ ions that occupy interstitial positions and the neighbor Li^+ on normal sites displaces the neighboring normal-site of Li^+ from the centers of the sites, thus reducing the potential barrier for Li^+ ions migration. As a result, at 300°C solid solutions of $\text{Li}_{6.15}\text{Zr}_{1.85}\text{Y}(\text{In})_{0.15}\text{O}_4$ have a lower conductivity compared to the solid electrolytes studied in the present work, however, at lower temperatures they will apparently have an advantage.

Table 3. Transport properties of some solid electrolytes based on lithium zirconates.

Solid Electrolyte	σ_{Li^+} , (S cm^{-1}) at 300 °C	E_a , (eV)
$\text{Li}_{5.8}\text{Zr}_{1.8}\text{Ta}_{0.2}\text{O}_7$, this work	6.92×10^{-3}	1.01
$\text{Li}_{5.8}\text{Zr}_{1.8}\text{Nb}_{0.2}\text{O}_7$, this work	3.16×10^{-3}	1.01
$\text{Li}_{1.85}\text{Ca}(\text{Zn})_{0.075}\text{ZrO}_3$ [34]	$\sim 10^{-5}$	0.85
$\text{Li}_{1.95}\text{Zr}_{0.95}\text{Nb}_{0.05}\text{O}_3$ [34]	4×10^{-6}	1.20
$\text{Li}_{2.05}\text{Zr}_{0.95}\text{Y}_{0.05}\text{O}_3$ [34]	10^{-6}	1.24
$\text{Li}_{5.6}\text{Mg}_{0.2}\text{Zr}_2\text{O}_7$ [22]	10^{-4}	0.95
$\text{Li}_{7.98}\text{Zr}_{0.98}\text{V}_{0.02}\text{O}_6$ [35]	3.7×10^{-5}	1.03
$\text{Li}_{7.85}\text{Mg}_{0.075}\text{ZrO}_6$ [20]	3.5×10^{-5}	0.85
$\text{Li}_{6.15}\text{Zr}_{1.85}\text{Y}_{0.15}\text{O}_7$ [24]	8.0×10^{-4}	0.63
$\text{Li}_{6.15}\text{Zr}_{1.85}\text{In}_{0.15}\text{O}_7$ [24]	6.4×10^{-4}	0.69

Vacancy solid solutions in Table 3 display the following pattern: solid electrolytes with substitutions in lithium sublattice ($\text{Li}_{1.85}\text{Ca}(\text{Zn})_{0.075}\text{ZrO}_3$, $\text{Li}_{5.6}\text{Mg}_{0.2}\text{Zr}_2\text{O}_7$, $\text{Li}_{7.85}\text{Mg}_{0.075}\text{ZrO}_6$) have a rather lower activation energy compared to the solid electrolytes with substitution of Zr^{4+} by Nb^{5+} or Ta^{5+} . This can be explained by the influence of the size factor. Activation energy depends on the mobility of the carriers, which, in its turn, depends on the size of crystallographic channels for Li^+ ions migration. The change of channel dimensions that accompanies heterovalent substitutions depends on the substituted ion and dopant radii. Li^+ and double charged ions (Mg^{2+} , Zn^{2+}) have rather close values of ionic radii (0.90, 0.86 and 0.88 Å, respectively [33]). Therefore, the substitution of Li^+ by Mg^{2+} or Zn^{2+} has no significant effect on the mobility of lithium ions. In contrast, Nb^{5+} and Ta^{5+} ions ($r = 0.78$ Å) are smaller than Zr^{4+} ($r = 0.86$ Å), so substitution of zirconium by niobium or tantalum leads to a significant decrease in cell volume (Figure 8) and, therefore, in the average radii of channels, which hinders Li^+ migration and increases the activation energy. However, the maximum dopant solubility in the case of doping $\text{Li}_6\text{Zr}_2\text{O}_7$ by double charged cations is far less compared to the solubility of the pentavalent ions, so the ionic conductivity of the former is smaller (Table 3).

High lithium-cation conductivity of solid solutions in $\text{Li}_{6-x}\text{Zr}_{2-x}\text{Nb}(\text{Ta})_x\text{O}_7$ systems can be assigned to a relatively open framework structure of the monoclinic $\text{Li}_6\text{Zr}_2\text{O}_7$ [23] and, compared to other lithium zirconates, a rather high solubility of the dopants, and, consequently, a higher concentration of charge carriers. Nevertheless, compared to the best solid lithium-cation conductors [36], the conductivity of the materials under study is relatively low, therefore, they can be used as solid electrolytes in LIBs only together with additional means of reducing the internal resistance of the battery, e.g., by using solid electrolytes in the form of thin films.

4. Conclusions

In the present work, solid lithium-cation electrolytes in $\text{Li}_{6-x}\text{Zr}_{2-x}\text{A}_x\text{O}_7$ ($\text{A} = \text{Nb}, \text{Ta}$) systems with $0 \leq x \leq 0.30$ have been synthesized. The electrolytes hold the monoclinic structure of $\text{Li}_6\text{Zr}_2\text{O}_7$ when $x \leq 0.25$. The monoclinic modification of $\text{Li}_6\text{Zr}_2\text{O}_7$ has been shown to exhibit better transport properties compared to the triclinic one. Temperature (300–600 °C) and concentration dependences of conductivity have been studied for the synthesized materials, their transport properties have been compared with the properties of other lithium zirconate-based solid electrolytes. Solid solutions of $\text{Li}_{5.80}\text{Zr}_{1.80}\text{Nb}(\text{Ta})_{0.20}\text{O}_7$ composition have a higher lithium-cation conductivity at 300 °C compared to solid electrolytes based on other lithium zirconates and to $\text{Li}_6\text{Zr}_2\text{O}_7$ -based solid solutions yielded by doping $\text{Li}_6\text{Zr}_2\text{O}_7$ with double- or triple-charged cations. The high conductivity of the solid solutions under study is related to the “open” structure of monoclinic $\text{Li}_6\text{Zr}_2\text{O}_7$ and high solubility of the doping five-charged cations which provides a high concentration of

lithium vacancies. It should be noted, however, that, even though the conductivity of solid electrolytes obtained in this work exceeds the conductivity of Li_2ZrO_3 - and Li_8ZrO_6 -based solid solutions, it remains relatively low compared to the best solid lithium-cation conductors, therefore, if the solid solution studied in this paper are to be used as electrolytes in all-solid-state LIBs, the internal resistance of the battery should be reduced by additional means, e.g., by using solid electrolytes in the form of thin films. Additionally, such solid solutions can be used as construction and electrode materials due to their thermodynamic stability in contact with metallic lithium.

Author Contributions: Conceptualization, G.S.S.; data curation, A.V.K.; formal analysis, B.D.A.; investigation, G.S.S.; visualization, A.V.K.; writing—original draft, G.S.S. All authors have read and agreed to the published version of the manuscript.

Funding: The research has been carried out in accordance with the budget plan of The Institute of High Temperature Electrochemistry, Ural Branch of the Russian Academy of Sciences (project No AAAA-A19-119020190042-7).

Institutional Review Board Statement: Not applicable.

Informed Consent Statement: Not applicable.

Data Availability Statement: The data presented in this study are available on request from the corresponding author.

Acknowledgments: The research has been partially carried out with the equipment of the Shared Access Center Composition of Compounds, Institute of High Temperature Electrochemistry, Ural Branch RAS, Ekaterinburg, Russian Federation.

Conflicts of Interest: The authors declare no conflict of interest.

References

1. Johnson, C.E.; Noda, K.; Roux, N. Ceramic breeder materials: Status and needs. *J. Nucl. Mater.* **1998**, *258*, 140–148. [[CrossRef](#)]
2. Avila, R.E.; Peña, L.A.; Jimenez, J.C. Surface desorption and bulk diffusion models of tritium release from Li_2TiO_3 and Li_2ZrO_3 pebbles. *J. Nucl. Mater.* **2010**, *405*, 244–251. [[CrossRef](#)]
3. Katsui, H.; Nagata, S.; Tsuchiya, B.; Shikama, T. Hydrogen trapping and luminescence characteristic in ion-implanted Li_2TiO_3 and Li_2ZrO_3 . *Nucl. Instrum. Methods Phys. Res.* **2012**, *272*, 275–279. [[CrossRef](#)]
4. Duan, Y. Electronic, Structural and electrochemical properties of lithium zirconates and their capabilities of CO_2 capture: A first-principles density-functional theory and phonon dynamics approach. *J. Renew. Sustain. Energy* **2011**, *3*, 013102. [[CrossRef](#)]
5. Yin, X.-S.; Song, M.; Zhang, Q.-H.; Yu, J.-G. High-Temperature CO_2 Capture on $\text{Li}_6\text{Zr}_2\text{O}_7$: Experimental and Modeling Studies. *Ind. Eng. Chem. Res.* **2010**, *49*, 6593–6598. [[CrossRef](#)]
6. Hellstrom, E.E.; Van, G.W. Constraints for the selection of lithium solid electrolytes. *Rev. Chim. Miner.* **1980**, *17*, 263–282.
7. Dong, Y.; Zhao, Y.; Duan, H.; Huang, J. Electrochemical performance and lithium-ion insertion/extraction mechanism studies on the novel Li_2ZrO_3 anode materials. *Electrochim. Acta* **2015**, *161*, 219. [[CrossRef](#)]
8. Miao, X.; Ni, H.; Zhang, H.; Wang, C.; Fang, J.; Yang, G. Li_2ZrO_3 coated $_{0.4}\text{Li}_2\text{MnO}_3\cdot_{0.6}\text{LiNi}_{1/3}\text{Co}_{1/3}\text{Mn}_{1/3}\text{O}_2$ for high performance cathode material in lithium-ion battery. *J. Power Sour.* **2014**, *265*, 147. [[CrossRef](#)]
9. Yi, H.; Wang, X.; Ju, B.; Shu, H.; Wen, W.; Yu, R.; Wang, D.; Yang, X. Effective enhancement of electrochemical performance for spherical spinel LiMn_2O_4 via Li-ion conductive Li_2ZrO_3 coating. *Electrochim. Acta* **2014**, *134*, 143. [[CrossRef](#)]
10. Huang, S.; Wilson, B.E.; Wang, B.; Fang, Y.; Buffington, K.; Stein, A.; Truhlar, N.G. Y-doped Li^8ZrO^6 : A Li-Ion Battery Cathode Material with High Capacity. *J. Am. Chem. Soc.* **2015**, *137*, 10992–11003. [[CrossRef](#)]
11. Huang, S.; Wilson, B.; Smyrl, W.H.; Truhlar, D.G.; Stein, A. Transition-Metal-Doped M-LiZrO (M = Mn, Fe, Co, Ni, Cu, Ce) as High-Specific-Capacity Li-Ion Battery Cathode Materials: Synthesis, Electrochemistry, and Quantum Mechanical Characterization. *Chem. Mater.* **2016**, *28*, 746. [[CrossRef](#)]
12. Hellstrom, E.; Van, G.W. Lithium-ion conduction in Li_2ZrO_3 , Li_4ZrO_4 and LiScO_2 . *Solid State Ion.* **1981**, *2*, 59. [[CrossRef](#)]
13. Murthy, S.R.A.; Gnanasekaran, T.; Jayaraman, V. Preparation and characterization of some lithium-ion conductors. *Solid State Ion.* **2017**, *303*, 138. [[CrossRef](#)]
14. Martel, L.C.; Roth, R.S. Phase-equilibria and crystal-chemistry in ternary oxide system containing $\text{Li}_2\text{O}-\text{MO}_2-\text{Ta}_2\text{O}_5$ (M = Ti, Sn, Zr, Th). *Am. Ceram. Soc. Bull.* **1981**, *60*, 376.
15. Vyders, G.P.; Cordfunke, E.H.P. Phase relations in the system $\text{Li}_2\text{O}-\text{ZrO}_2$. *J. Nucl. Mater.* **1989**, *168*, 24–30.
16. Delmas, C.; Maazaz, A.; Guillen, F.; Fouassier, C.; Reau, J.M.; Hagenmuller, P. Des conducteurs ioniques pseudo-bidimensionnels: Li_8MO_6 (M = Zr, Sn), Li_7LO_6 (L = Nb, Ta) et $\text{Li}_6\text{In}_2\text{O}_6$. *Mat. Res. Bull.* **1979**, *14*, 619. [[CrossRef](#)]

17. Andreev, O.L.; Pantyukhina, M.I.; Antonov, B.D.; Batalov, N.N. Synthesis and Electrical Properties of Lithium Metazirconate. *Russ. J. Electrochem.* **2000**, *36*, 1335. [[CrossRef](#)]
18. Pantyukhina, M.I.; Andreev, O.L.; Antonov, B.D.; Batalov, N.N. Electrical Properties of Lithium Zirconates. *Russ. J. Inorg. Chem.* **2002**, *47*, 1778.
19. Zou, Y.; Petric, A. Preparation and Properties of Yttrium-Doped Lithium Zirconate. *J. Electrochem. Soc.* **1993**, *140*, 1389–1392. [[CrossRef](#)]
20. Shchelkanova, M.S.; Pantyukhina, M.I.; Kalashnova, A.V.; Plaksin, S.V. Electrochemical properties of $\text{Li}_{8-2x}\text{M}_x\text{ZrO}_6$ (M = Mg, Sr) Solid electrolytes. *Solid State Ion.* **2016**, *290*, 12–17. [[CrossRef](#)]
21. Enriquez, L.J.; Quintana, P.; West, A.R. Compound Formation in the System $\text{Li}_2\text{O-ZrO}_2$. *Trans. Brit. Ceram. Soc.* **1982**, *81*, 17–19.
22. Kalashnova, A.V.; Shekhtman, G.S. Lithium cation conductivity of solid solutions in $\text{Li}_{6-2x}\text{M}_x\text{Zr}_2\text{O}_7$ (M = Mg, Ca, Zn) systems. *Alloy. Compd.* **2021**, *850*, 156809. [[CrossRef](#)]
23. Prasada, R.R.; Reddy, M.V.; Adams, S.; Chowdari, B.V.R. Preparation and mobile ion transport studies of Ta and Nb doped $\text{Li}_6\text{Zr}_2\text{O}_7$ Li-fast ion conductors. *Mater. Sci. Eng.* **2012**, *177*, 100–105.
24. Liao, Y.; Singh, P.; Park, K.S.; Li, W.; Goodenough, J.B. $\text{Li}_6\text{Zr}_2\text{O}_7$ interstitial lithium-ion solid electrolyte. *Electrochim. Acta* **2013**, *102*, 446–450. [[CrossRef](#)]
25. Abrahams, I.; Lightfoot, P.; Bruce, P.G. $\text{Li}_6\text{Zr}_2\text{O}_7$, a New Anion Vacancy ccp Based Structure Determined by ab initio Powder Diffraction Method. *J. Solid State Chem.* **1993**, *104*, 397–403. [[CrossRef](#)]
26. Pfeiffer, H.; Bosch, P. Thermal Stability and High-Temperature Carbon Dioxide Sorption on Hexa-lithium Zirconate ($\text{Li}_6\text{Zr}_2\text{O}_7$). *Chem. Mater.* **2005**, *17*, 1704–1710. [[CrossRef](#)]
27. Czekalla, R.; Jeitschko, W. Preparation and Crystal Structure $\text{Li}_6\text{Zr}_2\text{O}_7$ and $\text{Li}_6\text{Hf}_2\text{O}_7$. *Z. Anorg. Allg. Chem.* **1993**, *619*, 2038–2042. [[CrossRef](#)]
28. Rietveld, H.M. A profile refinement method for nuclear and magnetic structures. *J. Appl. Crystallogr.* **1969**, *2*, 65–71. [[CrossRef](#)]
29. Zocchi, M.; Natali, S.I.; Depero, L.E.; Roth, R.S. A Single Crystal X-ray Diffraction Study of Lithium Zirconate $\text{Li}_6\text{Zr}_2\text{O}_7$, a Solid-State Ionic Conductor. *J. Solid State Chem.* **1993**, *104*, 391–396. [[CrossRef](#)]
30. Nan, C.-W. Physics of Inhomogeneous Inorganic Materials. *Prog. Mater. Sci.* **1993**, *37*, 1–116. [[CrossRef](#)]
31. Villafuerte, C.M.E.; Kuhliger, C.; Ovando, R.; Smith, R.I.; West, A.R. New Perovskite Phases in the Systems $\text{Li}_2\text{O-(Nb}_2\text{O}_5, \text{Ta}_2\text{O}_5)\text{-ZrO}_2$. *J. Mater. Chem.* **1991**, *1*, 747–749. [[CrossRef](#)]
32. Lightfoot, P.; Tomson, J.B.; Little, F.J.; Bruce, P.G. Ab Initio Determination of Crystal Structures by X-Ray Powder Diffraction: Structure of $\text{Li}_{29}\text{Zr}_9\text{Nb}_3\text{O}_{40}$. *J. Mater. Chem.* **1994**, *4*, 167–169. [[CrossRef](#)]
33. Shannon, R.D. Revised effective ionic radii and systematic studies of interatomic distances in halides and chalcogenides. *Acta Cryst.* **1976**, *32*, 751–767. [[CrossRef](#)]
34. Kalashnova, A.V.; Plaksin, S.V.; Shekhtman, G.S. Effect of Dopants on the Lithium Metazirconate Conductivity. *Russ. J. Electrochem.* **2020**, *56*, 500–510. [[CrossRef](#)]
35. Shchelkanova, M.S.; Shekhtman, G.S.; Kalashnova, A.V.; Reznitskikh, O.G. Lithium ion conductivity of solid solutions based on Li_8ZrO_6 . *J. Solid State Electrochem.* **2018**, *22*, 2959–2964. [[CrossRef](#)]
36. Bachman, J.C.; Muy, S.; Grimaud, A.; Chang, H.H.; Pour, N.; Lux, F.S.; Paschos, O.; Maglia, S.; Lupart, S.; Lamp, P.; et al. Inorganic Solid-State Electrolytes for Lithium Batteries: Mechanisms and Properties Governing Ion Conduction. *Chem. Rev.* **2016**, *116*, 140–162. [[CrossRef](#)]